IRAQI JOURNAL OF APPLIED PHYSICS
Vol. 22, No. 1, January-March 2026, pp. 19-23

Characterization of Aluminum-Doped Titanium Dioxide Thin Films Prepared by Pulsed-Laser Deposition

Abdulrahman A. Abdulazez
Kawkab D. Salim

Department of Physics,
College of Education for
Pure Sciences,
University of Tikrit,
Tikrit, IRAQ
* Corresponding author:
AA230058pep@st.tu.edu.iq

Enhancing structural and optical characteristics is essential for optimizing the performance of thin-film applications. This work examines the creation of thin films of pure titanium dioxide (TiO2) included with 2% and 4% aluminum, which were subjected to heating post-deposition on glass and produced via the pulsed laser deposition technique. X-ray diffraction (XRD) analysis revealed a distinctive TiO2 (103) peak at 2Θ = 36.91°. The crystal structure of TiO2 is characterized as rutile. Atomic force microscopy (AFM) images indicated that the heat treatment led to a reduction in the grain size of both the pure and doped films, resulting in an increased surface roughness. SEM images additionally demonstrated pure TiO2 sheets integrated with aluminum (Al). The images indicated that the atoms were uniformly scattered, with some aggregating into grape-like clusters. The energy gap dropped from 3.47 eV to 3.36 eV with changes in doping ratios.

Keywords: Thin films; Pulsed-laser deposition; Titanium dioxide; Optical properties
Received: 14 May 2025; Revised: 30 June; Accepted: 7 July 2025; Published: 1 January 2026

1. Introduction

Thin films consist of one or more layers of materials with diameters ranging from 1 to 100 nanometers [1]. The term of "thin films" refers to a layer or many layers of material atoms with thicknesses varying from several nanometers to one micrometer. Due to their fragility, thin films are deposited on robust materials such as glass, metal, polymers, and other solid substrates. Thin films possess various intrinsic features, including their crystalline structure and thickness. The configuration of thin films is contingent upon the preparation method, potentially yielding either random single or polycrystalline films. Moreover, alterations in their optical and electrical characteristics are contingent upon their crystalline structure and the presence or absence of impurities [2]. The objective of depositing these films is to safeguard them against harm and to acquire new qualities, including alterations in their structural and electrical characteristics [3]. Thin films are utilized throughout diverse domains, including industry and engineering, as well as in electronic applications such as magnetic memory, switching circuits, resistors, amplifiers, detectors, solar cells, and radiation sensors [4]. Reflective coatings, anti-reflective coatings, interference filters, and cutoff filters utilize thin films [4,5]. Numerous techniques for fabricating thin films have developed alongside scientific progress, attaining a high level of accuracy in measuring film thickness and uniformity. The selection of a preparation process is contingent upon various aspects, such as the film's intended application, the material utilized, and the associated preparation costs [6,7]. Preparation procedures encompass physical approaches, including evaporation methods (e.g., laser evaporation, flash evaporation, and radiofrequency heating) and sputtering methods (e.g., reactive sputtering and DC sputtering). Chemical approaches encompass thermal chemical spraying and colloidal solution deposition [8]. Pulsed-laser deposition (PLD) is the technique employed in this research for the creation of thin films. PLD is a straightforward method that depends on the interaction between a high-energy laser beam and the target substance. This method comprises three primary elements: the laser, the pumping mechanism, and the chamber [9]. The laser beam is incident on the target material, and if the energy density exceeds the threshold, the material is ablated from the target surface [10]. This approach is applicable to a range of materials, including electrical insulators, semiconductors, metals, organic substances, and polymers [11]. This research will apply this approach to titanium dioxide (TiO_2), the substance utilized in this investigation. Titanium dioxide is prevalent in nature, positioned eighth among the elements in the Earth's crust. It has numerous functions, including imparting whiteness or opacity in items such as paper, paints, plastics, and toothpaste [12]. We also offer TiO_2 in powdered form for use as a pigment, commonly known as titanium white or white pigment. Other oxides or metals combine with TiO_2, which does not exist in its pure state. It is an n-type semiconductor with an energy bandgap of 3.04 to 3.64 eV [13]. TiO_2 is white and devoid of odor [14] and can be found in three natural forms: anatase, rutile,

and brookite, with anatase and rutile being the most common, and both have a four-sided crystal shape [15]. The brookite phase is infrequent [16].

2. Experimental Part

High-purity (99.999%) titanium dioxide and aluminum powders were used. Titanium dioxide (TiO_2) was used as the substrate, with aluminum added at 2% and 4% weights. To complete the deposition process, the glass substrates were immersed in a vat of pure acetone (99%) to remove any residual grease or surface particles. Then, they were cleaned with distilled water and subjected to an ultrasonic cleaner for 15 minutes. The mixing ratios were determined using the molecular weights of aluminum and titanium. The components were mixed in an agate mill for 30 minutes, then transferred to a 12mm diameter steel mold and subjected to a 4-ton pressure for 10 minutes until the hydraulic press stabilized. A 4mm-thick target was fabricated and then placed in a thermal oven at 100°C for 1 hour to homogenize the components and remove moisture from the target. A pulsed Nd:YAG laser with a pulse duration of 10 ns, a wavelength of 1064 nm, an output energy of 800 mJ, a frequency of 6 Hz, and a pulse count of 900 pulses, was used to prepare the films. The target was positioned 2 cm below the glass base to ensure optimal homogeneity during the ablation process. The chamber was evacuated to a pressure of 10^{-3} torr, and the laser beam was directed toward the target at a 45° angle with 900 pulses. The samples were then heated to 400°C for 30 minutes. Figure (1) shows a pictorial summary of the method of preparing pure TiO_2 films those were doped with aluminum.

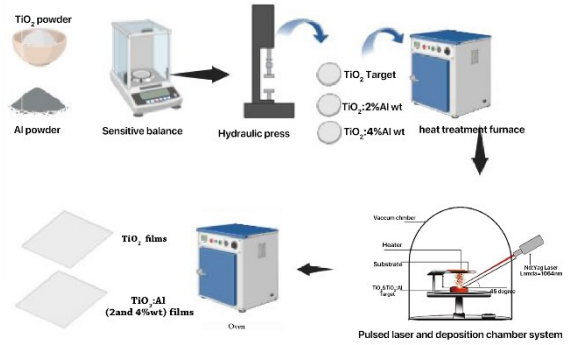

Fig. (1) Schematic diagram of the steps involved in thin film preparation

3. Results and Discussion

Figure (2) illustrates the X-ray diffraction (XRD) patterns of pure TiO_2 films and those doped with aluminum (Al) at weight concentrations of 2% and 4%, produced via PLD. The results indicated a TiO_2 peak at the (103) plane corresponding to an angle of $2\theta = 36.91°$, aligning with the ICDD standard card 01-070-7348, as presented in table (1). This is the favored alignment for all ratios. The TiO_2 films exhibit a rutile crystal structure. The Al-doped TiO_2 film exhibited three peaks at the (110), (111), and (211) planes, with angles $2\theta = 27.94°$, 41.92°, and 54.90°, respectively, in accordance with the ICDD standard card 01-077-0441, as presented in table (1). All films are polycrystalline structures. Aluminum doping enhanced the crystal structure and augmented the uniformity of the material by occupying vacancies and rectifying crystal faults [17]. The full-width at half maximum (FWHM) of the peaks was noted to grow with higher doping ratios, signifying a reduction in grain size. The crystallite size (D) was determined using Scherrer's equation:

$$D = \frac{0.9\lambda}{\beta cos\theta} \qquad (1)$$

revealing a reduction in grain size with higher doping ratios, as indicated in table (1)

A little displacement in the peak positions toward smaller angles was noted as a result of doping, since impurities significantly influence the crystal structure of the films, leading to a shift in the peak positions toward decimal values, in accordance with [18].

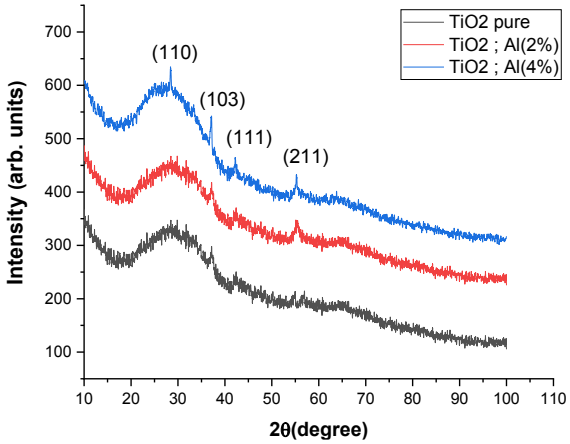

Fig. (2) XRD patterns of pure and Al-doped TiO_2 thin films

Figure (3) presents the atomic force microscopy (AFM) results for pure and Al-doped TiO_2 films. These results depicts the grain distribution on the film's surface. The grain size diminishes with higher doping ratios, with measurements ranging from 81.645 nm to 70.462 nm, as illustrated in table (2). The average surface roughness and root mean square (RMS) values decreased as the doping ratios increased, going from 14.402 nm to 8.543 nm and from 19.103 nm to 11.926 nm, respectively. Examining film surfaces is important when studying the arrangement and distribution of atoms at the surface level. Prominent grains on the film surface signify a degradation of the crystal structure, aligning with [19]. The photos depict the configurations of the grains, resembling mountains or pyramids.

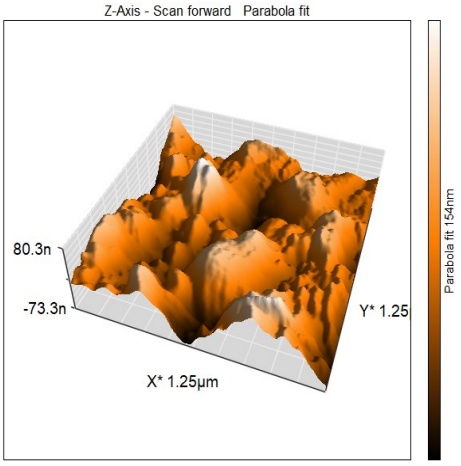

Pure TiO_2

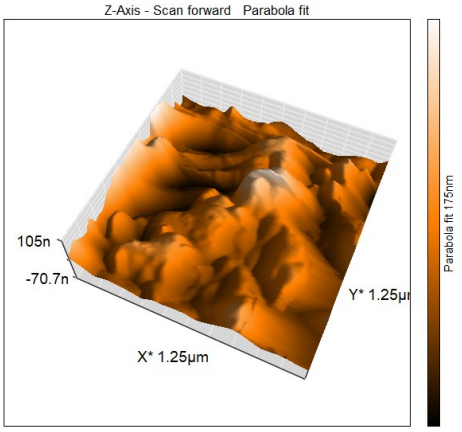

2% Al

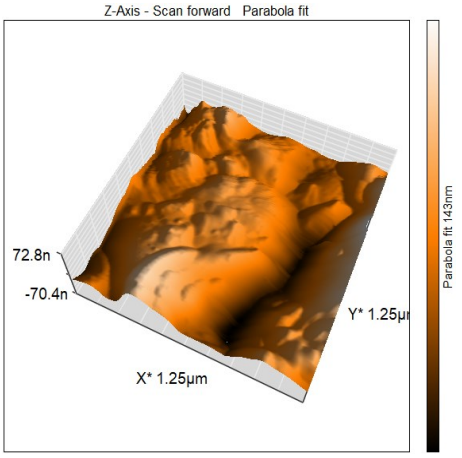

4% Al

Fig. (3) AFM images of pure and Al-doped TiO_2 thin films

Table (2) Values of average roughness (R_{ave}), root-mean-square roughness (R_{RMS}), and average grain size (D_{ave}) obtained from AFM results

Sample	R_{ave} (nm)	R_{RMS} (nm)	D_{ave} (nm)
Pure TiO_2	14.402	19.103	81.645
2% AL-doped TiO_2	12.676	17.273	78.246
4% Al-doped TiO_2	8.543	11.926	70.462

Figures (4-6) show scanning electron microscope (SEM) images at 500 nm magnification of pure and Al-doped TiO_2 films prepared in this work. The image in Fig. (4) demonstrates the proliferation and dispersion of particles exhibiting quasi-spherical configurations of various dimensions, resembling grape clusters. The average particle size ranges from 56 to 70 nm. Figure (5) presents SEM images of 2% Al-doped TiO_2 film. The addition of aluminum alters the particle morphology, making the particles denser and smaller than those in the pure film, which implies a smoother surface due to the added impurities. The average particle size ranges from 41 to 52 nm. Figure (6) presents SEM images of 4% Al-doped TiO_2 film. The image changes as a result of the addition of aluminum, making them darker than those in the pure film and dispersing them more evenly. The average particle size is ranging between 36 and 48 nm [20].

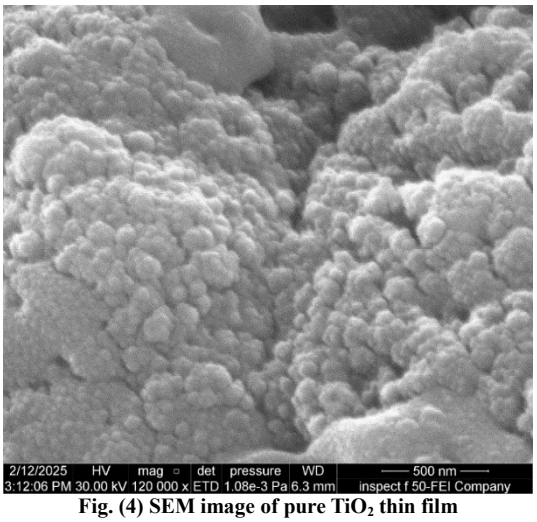

Fig. (4) SEM image of pure TiO_2 thin film

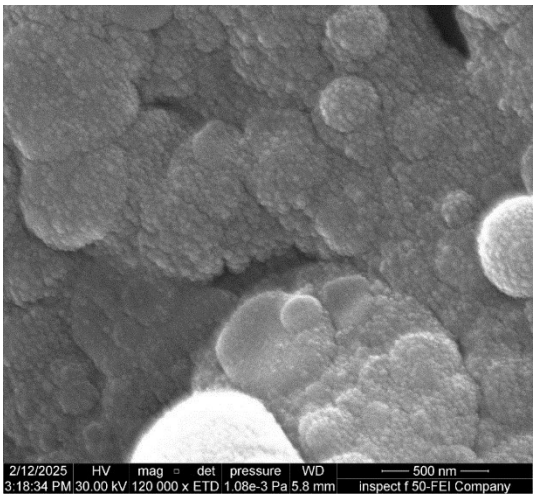

Fig. (5) SEM image of 2% Al-doped TiO_2 thin film

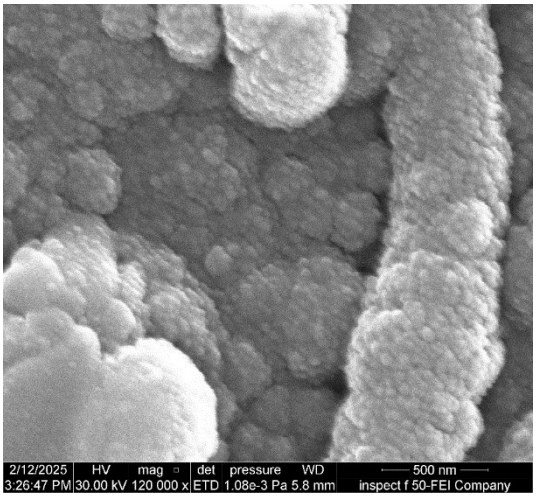

Fig. (6) SEM image of 4% Al-doped TiO_2 thin film

Absorption spectra of the pure and Al-doped TiO_2 films were recorded in the wavelength range of 190-1100 nm. The energy gap was determined from the absorption spectral data using the correlation between the allowed direct transition $(\alpha h\upsilon)^2$ and photon energy $(h\upsilon)$ as:

$$\alpha h\nu = B_0\left(h\nu - E_g^{opt}\right)^r \qquad (2)$$

where B_0 is essentially a constant, Eg^{opt} is the optical energy band gab and $r = 1/2$ for the allowed transition

Figure (7) shows an increase in absorbance with increasing doping ratios. This increase is attributed to the impurity levels formed by aluminum (Al) atoms in the base material (TiO_2) between the valence and conduction bands. The laser power and the number of pulses used in the deposition process also play a role, as increasing the laser power and the number of pulses increases the ablation of particles from the target material, in accordance with. The graphs of energy band gap for pure and Al-doped TiO_2 films show that as the amount of aluminum increases, the energy gap value decreases from 3.447 to 3.359 eV, as seen in table (3) [21,22]. The energy band gap gets narrower because adding more aluminum creates extra energy levels between the valence and conduction bands, which lets electrons move more easily from the valence band to the conduction band. Many parameters can influence the energy band gap, such as the type of film material, how it is made, the doping level, the conditions during preparation, and the structure and order of the films that are made, according to reference [23].

Table (3) Values of energy band gap for pure and Al-doped TiO_2 films

Sample	Energy band gap (eV)
Pure TiO_2	3.47
2% Al-doped TiO_2	3.39
4% Al-doped TiO_2	3.36

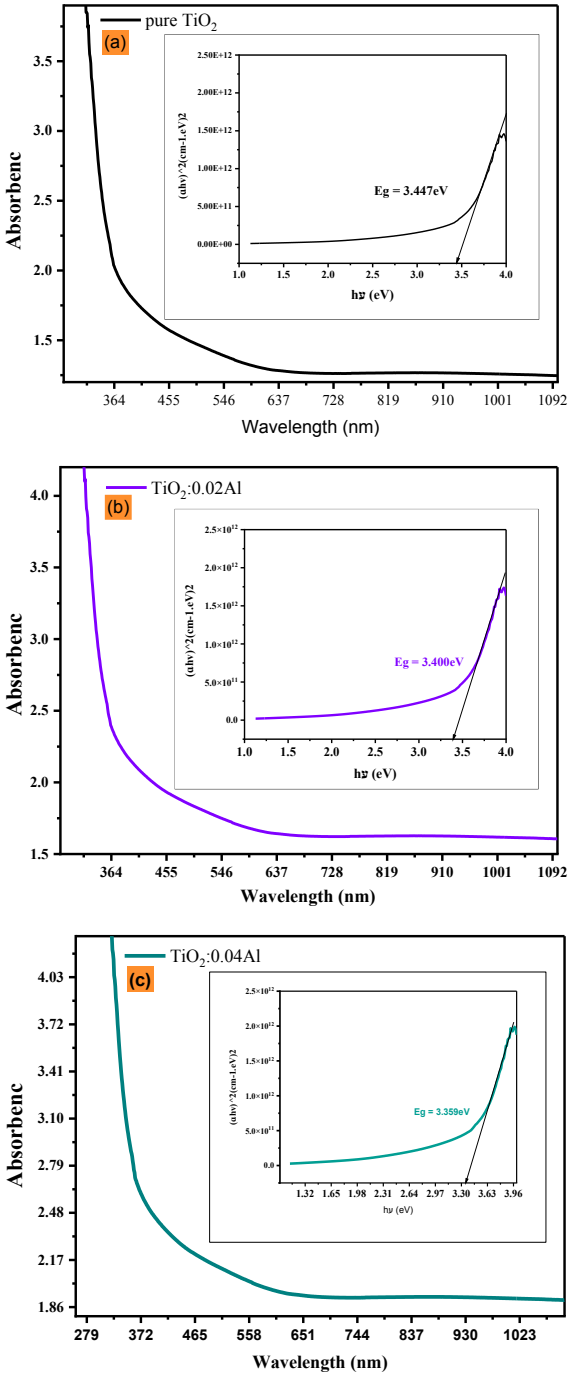

Fig. (7) UV-visible absorption spectra and optical energy gap results for (a) pure TiO_2, (b) 2% Al-doped TiO_2, and (c) 4% Al-doped TiO_2 thin films

4. Conclusion

Pure TiO_2 thin films were prepared and doped with aluminum by pulsed-laser deposition. Aluminum doping showed improved optical and structural properties. The crystallite size was 12.1345 nm at the (103) crystal plane before doping and decreased upon doping at the same plane. The effect of doping on the prepared thin films was very noticeable on the surface roughness, which decreased to 8.54. Finally, the

doping process dominated the energy band gap value, which decreased to 3.359 eV.

References

[1] G. Shukla, P.K. Mishra and A. Khare, "Effect of annealing and O_2 pressure on structural and optical properties of pulsed laser deposited TiO_2 thin films", *J. Alloys Comp.*, 489(1) (2010) 246-251.

[2] A. El-Denglawey, M.M. Makhlouf and M. Dongol, "The effect of thickness on the structural and optical properties of nano Ge-Te-Cu films", *Res. in Phys.*, 10 (2018) 714-720.

[3] U.K. Mishra and J. Singh, **"Semiconductor device physics and design",** Dordrecht: Springer (2008), vol. 83.

[4] L. Eckortova, **"Physics of Thin Films",** Plenum Press (NY, 1977).

[5] H.G. Roshid, "Design and Optimization of Thin Film Optical Filters and Applications in the Visible and Infrared Regions", PhD thesis, Al-Mustansirya University (1996).

[6] L. Eckertova, **"Physics of thin films"**, Springer Science and Business Media (2012).

[7] H. Frey and H.R. Khan (eds.), **"Handbook of thin film technology",** Springer (Berlin, 2015).

[8] H.H. Wieder, "Intermetallic Semiconducting Films", International Series of Monographs in Semiconductors, vol. 10 (2014).

[9] E.G. Gamaly, A.V. Rode and B. Luther-Davies, **"Pulsed Laser Deposition of Thin Films Ultrafast Laser Ablation and Film Deposition"**, John-Wiley and Sons, Inc. (2006).

[10] D.M. Martín, "TeO_2-based film glasses for photonic applications: structural and optical properties", PhD dissertation, Universidad Complutense de Madrid (2009).

[11] Z. Roohi, F. Mighri and Z. Zhang, "Conductive Polymer-Based Electrodes and Supercapacitors Materials, Electrolytes, and Characterizations", *Materials*, 17(16) (2024) 4126.

[12] A.A. Hussain and Q.N. Abdullah, "Characterization of ZnO-SnO_2 Nanostructures Prepared by Thermal Evaporation Technique as Gas Sensor", *Iraqi J. Appl. Phys.*, 19(4C) (2023) 243-250.

[13] M. Walczak et al., "Structural and morphological characterization of TiO_2 nanostructured films grown by nanosecond pulsed laser deposition", *Appl. Surf. Sci.*, 255(10) (2009) 5267-5270.

[14] E. Francisco et al., "Spinodal equation of state for rutile TiO_2", *Phys. Rev. B*, 67 (2003) 064110.

[15] R.S. Rusu and G.I. Rusu, "On the electrical and optical characteristics of CdO thin films", *J. Optoelectron. Adv. Mater.*, 7(3) (2005) 1511-1516.

[16] W.J. Yin et al., "Excess electrons in reduced rutile and anatase TiO_2", *Surf. Sci. Rep.*, 73(2) (2018) 58-82.

[17] D.K. Calvo Ramos et al., "Obtaining and Characterization of TiO_2-GO Composites for Photocatalytic Applications", *Int. J. Photoener.*, 2020 (2020) 3489218.

[18] T. Raguram, K.S. and Rajni, "Influence of boron doping on the structural, spectral, optical and morphological properties of TiO_2 nanoparticles synthesized by sol–gel technique for DSSC applications", *Mater. Today*, 33(5) (2020) 2110-2115.

[19] T.H. Tsai, S.C. Chiou and S.M. Chen, "Enhancement of dye-sensitized solar cells by using graphene-TiO_2 composites as photoelectrochemical working electrode", *Int. J. Electrochem. Sci.*, 6(8) (2011) 3333-3343.

[20] S. Kumar, N.K. Verma and M.L. Singla, "Study on reflectivity and photostability of Al-doped TiO_2 nanoparticles and their reflectors", *J. Mater. Res.*, 28 (2013) 521-528.

[21] Z. Essalhi et al., "Optoelectronics properties of TiO_2:Cu thin films obtained by sol gel method", *Opt. Quant. Electron.*, 49 (2017) 301.

[22] M.K. Singh, and M.S. Mehata, "Phase-dependent optical and photocatalytic performance of synthesized titanium dioxide (TiO_2) nanoparticles", *Optik*, 193 (2019) 163011.

[23] N.M. Ravindra, P. Ganapathy and J. Choi, "Energy gap–refractive index relations in semiconductors–An overview", *Infrared Phys. Technol.*, 50(1) (2007) 21-29.

Table (1) X-ray diffraction results

Sample	2θ (Deg)	FWHM (Deg)	d_{hkl} Exp (Å)	Crystallite size D (nm)	(hkl)	d_{hkl} Std (Å)
Pure TiO_2	36.912	0.6214	2.4106	12.1345	103	2.4248
2% AL-doped TiO_2	36.730	0.6384	2.4115	11.7954	103	2.4248
	54.903	0.5235	1.6884	13.4608	211	1.6963
4% AL-doped TiO_2	36.641	0.6429	2.4107	11.7246	103	2.4248
	54.814	0.5346	1.6884	13.1752	211	1.6963
	41.921	0.3204	2.1917	23.1862	111	2.1995
	27.943	0.3624	3.2538	21.2716	110	3.2640

